Thermographic Crack Detection in Ferritic Steel Components Using Inductive Heating

Günter WALLE and Udo NETZELMANN,
Fraunhofer Institute for Nondestructive Testing, Saarbrücken, Germany

Abstract. Active dynamic thermography using inductive heating was used for investigations on different steel components from automotive and steel industry. The defects were perpendicular and slanted surface cracks. For the ferritic steel investigated in the study, the skin depth was usually smaller than the crack depth. Cracks with a depth down to 200 µm were detected. A theoretical model for the temperature profile around a crack resulting from a given induction field was set up and compared with experimental results. Both in model and in experiment, an almost linear dependence of the defect contrast on defect depth was found up to a depth of about 0.8 mm. The dependence of the contrast as a function of the crack orientation vs. the induction field was studied. In comparison to ultrasonically excited thermography, induction heating was applicable to a larger variety of specimen shapes and showed more crack indications.

1. Introduction

Dynamic thermography with inductive excitation is an interesting alternative to magnetic particle inspection or eddy current testing. A high frequency induction coil in the neighbourhood of the test object generates eddy currents. Crack detection is based on the changes of the distribution of the locally induced eddy currents due to the crack, which lead to locally changed eddy current losses near the cracks. Hence, a higher heat generation occurs near the crack which can be used for thermographic heat detection. Perpendicular cracks, but also slanted cracks can be detected in this way.

First applications in steel industry were more than two decades ago [1], where continuous inductive heating on moving steel bars was applied to detect longitudinal cracks. Further, the technique has been applied using periodic heating and phase sensitive detection for characterization of coating adhesion [2] and using pulsed excitation for crack detection in turbine blades [3,4]. Recently, new applications on steel components and CFRP [5] and analytical and numerical modelling of the signal from cracks were reported [6].

In this work, a model for heat generation by a crack in a bar including the inductive excitation is set-up and verified on different steel components from automotive industry.

2. Theoretical considerations

A two dimensional analytical model based on an infinitely long parallelepiped (in y-direction) with a width a and a height b was created [7]. It is assumed that due to an electromagnetic excitation of the specimen eddy currents will be induced, which generate an additional surface current density along the crack flanks as shown in Figs. 1 and 2. As the materials investigated here were magnetic, the skin depth was usually smaller than the

crack depth. The current density causes eddy current losses with a power density P in a thin layer. Due to these heat sources on the crack flanks an instationary heat flow is produced propagating into the bulk of the material and to the specimen surface. At a time t after the begin of the inductive excitation a temperature distribution T(z,t) is caused at the specimen surface ($x_0 = 0$), which can be detected by an infrared camera.

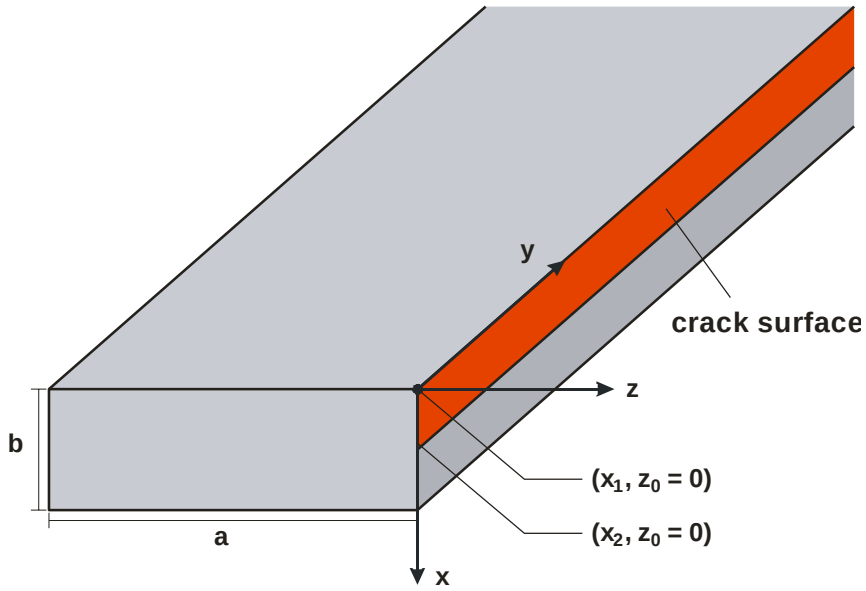

Figure 1: Geometry of the model (the symmetric right part of the sample is omitted)

The crack area (crack flank: red in Fig. 1) is oriented along the x-axis (z = 0) from $x = x_1$ to $x = x_2$ and in y-direction.

For the case that the heat sources due to the eddy current losses are active during the excitation time t_p, the temperature T at the surface (x = 0) along the z-axis is written as

$$T(z,t) = T_1 + T_2 + T_3\,, \tag{1}$$

where

$$T_1 = \frac{P}{\rho c a b}\left(t_p(x_2 - x_1) + \frac{2a^2(x_2 - x_1)}{\alpha\pi^2}\sum_{n=1}^{\infty}\frac{1}{n^2}e^{-n^2\beta_1 t}\left(e^{n^2\beta_1 t_p} - 1\right)\cos\left(n\pi\frac{z}{a}\right)\cos\left(n\pi\frac{z_0}{a}\right)\right), \tag{2}$$

$$T_2 = \frac{P}{\rho c a b}\frac{2b^2}{\alpha\pi^2}\sum_{m=1}^{\infty}\frac{1}{m^2}\frac{b}{m\pi}e^{-m^2\beta_2 t}\left(e^{m^2\beta_2 t_p} - 1\right)\cos\left(m\pi\frac{x_0}{b}\right)\cdot\left(\sin\left(m\pi\frac{x_2}{b}\right) - \sin\left(m\pi\frac{x_1}{b}\right)\right), \tag{3}$$

$$T_3 = \frac{P}{\rho c a b}\frac{4a^2b^2}{\alpha\pi^2}\sum_{n=1}^{\infty}\sum_{m=1}^{\infty}\left(\frac{1}{n^2b^2 + m^2a^2}\right)\left(\frac{b}{m\pi}\right)e^{-\beta_3 t}\left(e^{\beta_3 t_p} - 1\right)\cos\left(n\pi\frac{z}{a}\right)\cos\left(n\pi\frac{z_0}{a}\right) \cdot\cos\left(m\pi\frac{x_0}{b}\right)\left[\sin\left(m\pi\frac{x_2}{b}\right) - \sin\left(m\pi\frac{x_1}{b}\right)\right], \tag{4}$$

and

$$\beta_1 = \frac{\alpha\pi^2}{a^2}\,,\quad \beta_2 = \frac{\alpha\pi^2}{b^2}\,,\quad \beta_3 = \alpha\pi^2\left(\frac{n^2}{a^2} + \frac{m^2}{b^2}\right). \tag{5}$$

Here, ρ is the density of the material, c the specific heat capacity and α the thermal diffusivity.

2.1 Estimation of the power density P of the eddy current losses, producing the crack signal

Starting from Maxwell´s equations:

$$\int \vec{E}\,\vec{ds} = \int \frac{\vec{dB}}{dt}\vec{dA}\,,\quad \int \vec{H}\vec{ds} = \sigma \int \vec{J}\vec{dA}\,,\ \text{and}\ \vec{J} = \sigma\vec{E}\,,$$

where $\vec{E}$ is the electric field strength, $\vec{B}$ the magnetic flux density, $\vec{H}$ the magnetic field and $\vec{J}$ the current density, for a plate geometry (see Fig. 2; coordinate system according to Fig. 1) one finds for the absolute of the eddy current density [8]:

$$J = \beta\sqrt{2}H\frac{\sqrt{\cosh(2\beta x)-\cos(2\beta x)}}{\sqrt{\cosh(\beta b)+\cos(\beta b)}}\,, \qquad (6)$$

with $\beta = \sqrt{\pi f\sigma\mu} = 1/\delta$. Here, δ is the skin depth, b the plate thickness, f the eddy current excitation frequency, σ the electrical conductivity and μ the magnetic permeability of the material. It is assumed, that the crack is small enough to neglect its effect on the overall current distribution in the bar.

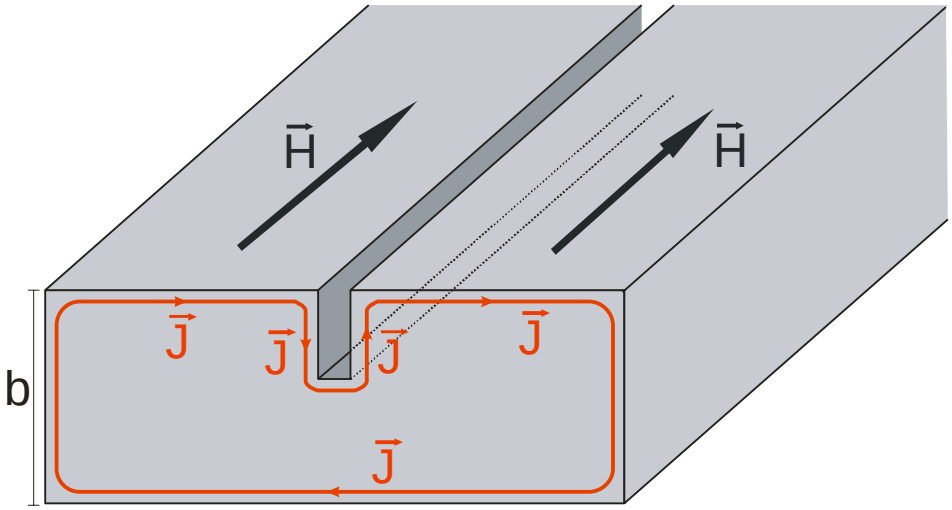

Fig. 2: Plate geometry with a crack and eddy currents

Eddy current losses:

The eddy current losses per unit area on the plate surface can be calculated from an integral over the square of the current density J:

$$P = 0.5\frac{1}{\sigma}\int J^2 dx \qquad (7)$$

For the case where the penetration depth of the eddy currents is much less than the plate thickness ($\delta << b$) the integration yields, using (6):

$$P = \beta H^2 / (2\sigma) \qquad (8)$$

This is the value of the power density of eddy current losses at the surface of the plate geometry (Fig. 2). Assuming that in the presence of a crack the eddy currents follow the crack along its flank areas (see Fig. 2) and assuming that the current density is the same as in the crack free case the eddy current losses at the crack flank areas are the same as calculated from (8).

For example, one finds for the parameters $f = 100$ kHz; $\sigma = 10^7$ 1/Ωm; $\mu = 100$:

$\beta = 19.9$ mm^{-1}

$\delta = 0.05$ mm

The plate thickness is assumed to be $b = 10$ mm. If we apply a magnetic field strength of the excitation of $H = 100$ A/cm, we finally obtain for the power density of the eddy current losses at the crack flanks:

$P = 10^5$ W/m^2.

2.2 Application of the model

We assume a crack starting at the surface $x_1 = 0$ with a depth of $x_2 = 0.8$ mm which is infinitely long (Fig. 1). Furthermore, we use the same parameters for frequency, electrical conductivity, magnetic permeability, magnetic field strength and plate thickness as before. So we obtain the eddy current loss power at the crack flanks as calculated before and using (1) the following result for the crack signal T(z, t) for an excitation time $t_p = 0.2$ s (Fig. 3).

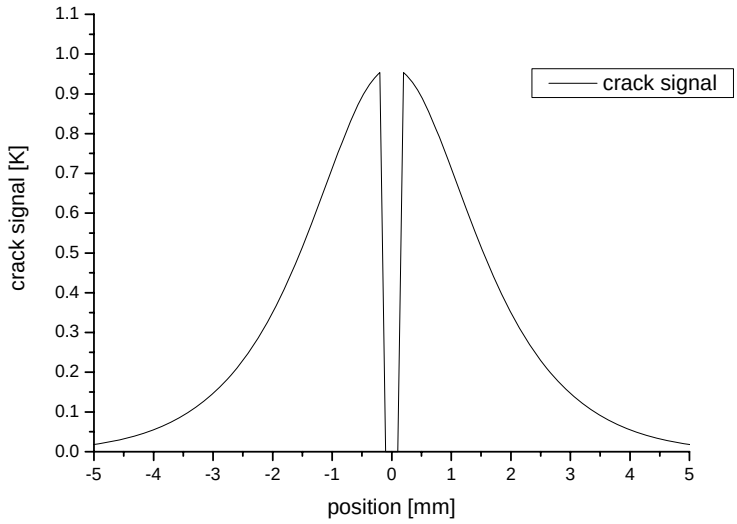

Fig. 3: Calculated crack signal of a 0.8 mm deep crack

This result compares well with results reported in [6]. If we calculate the signal curves for various crack depths under constant model parameters we obtain the following behaviour of the maximum crack signal as a function of the crack depth.

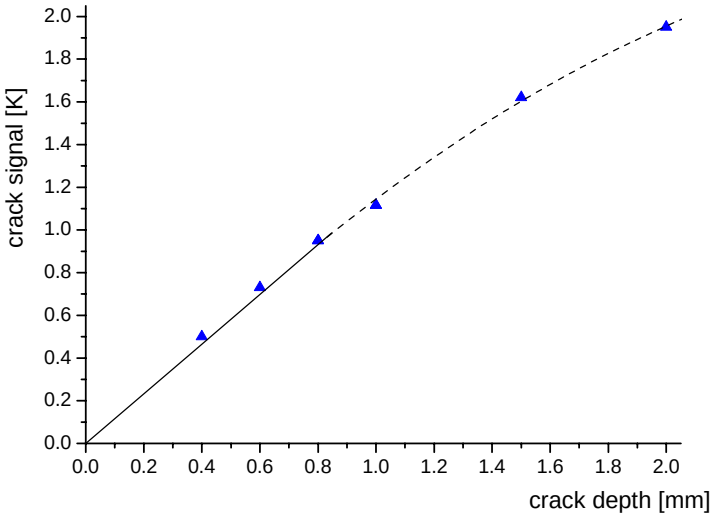

Fig. 4: Calculated dependence of the crack signal on crack depth

In the following, these results will be compared with experimental examinations.

3. Experimental results

3.1 Measurements for examining the dependence of the crack signal on defect depth

Measurements were performed using a ferromagnetic steel plate of the thickness of 10 mm with artificial cracks (saw cuts) of different depths (from 0.2 mm to 2.0 mm), a width of 0.2 mm and a length of 10 mm. The specimen was excited by an electromagnetic field with a frequency of about 100 kHz and a with magnetic field orientation as indicated in Fig. 2. For the case of an excitation time of 0.2 s we obtain the following result for the defect with a depth of 0.8 mm (Fig. 5). The defect clearly can be recognized in the thermographic image due to the characteristic temperature enhancement around the crack (at right of the arrow). In Fig. 5b the temperature signal of the crack (B, coded in binary output of the camera signal) along a line going through the arrow in Fig. 5a is presented.

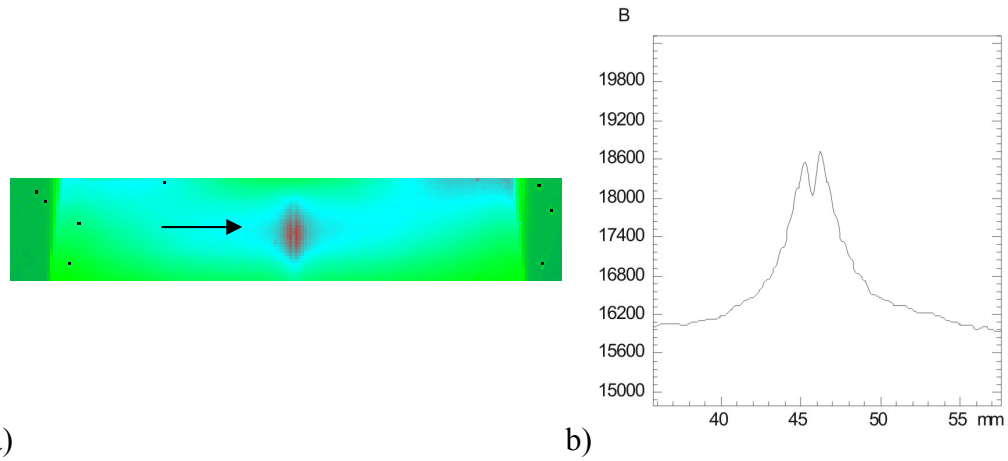

a) b)

Fig. 5: a) Thermographic image of the temperature distribution around the defect (at right from arrow). The depth of the crack is $x_2 = 0.8$ mm. b) Crack signal along the arrow line

The measurements at the other defects were made using the same parameters. For crack signal dependence on depth we find the following result (Fig. 6).

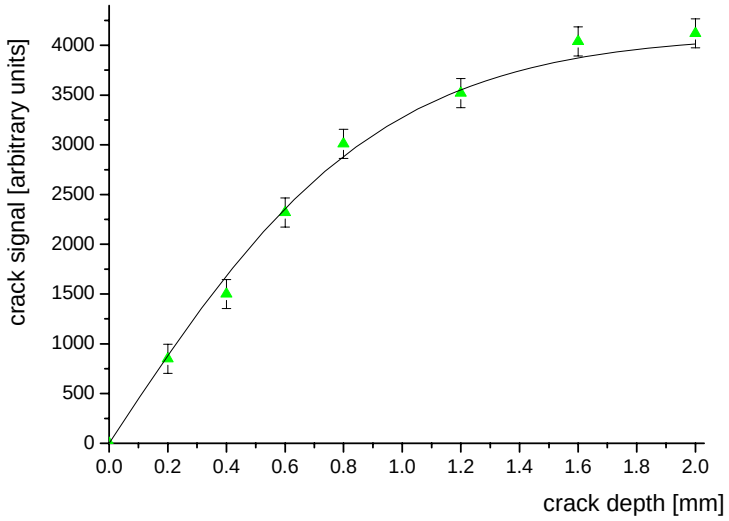

Fig. 6: Measured dependence of the crack signal on crack depth

A comparison between the measurement result and the result of model calculations shows that up to a defect depth of about 0.8 mm one finds a linear increase of the crack signal with defect depth. Then saturation behaviour is found in the measurement result as well as in the model calculations. But as one can see the saturation behaviour in the measurement is stronger than in the model calculation. This can be caused by the fact that in the measurements a finite crack length was given while in the calculations an infinite crack length was assumed. In further work, it is planned to investigate the influence of the defect geometry in more detail.

3.2 Examinations related to the influence of the orientation of the eddy currents with respect to crack orientation

The above investigations were performed under the condition that the eddy currents were oriented perpendicular to the crack orientation. In the following, we consider the dependence of the crack signal on various orientations of the eddy currents with respect to the crack orientation. The results of these measurements are shown in Fig. 7.

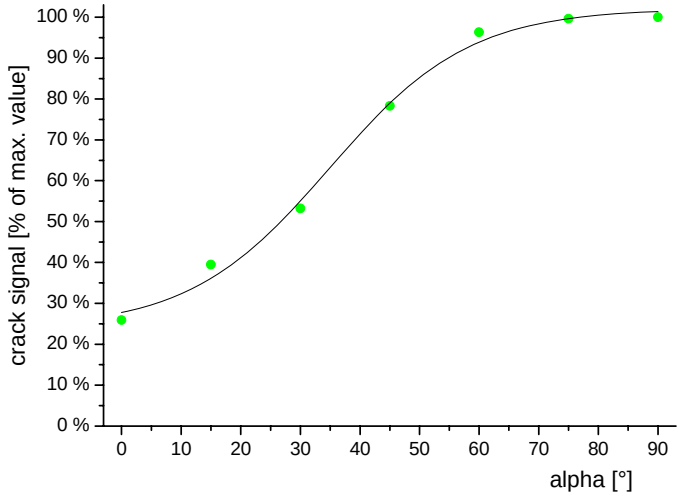

Fig. 7: Thermal crack signal as a function of the angle (alpha) of the eddy currents with respect to crack orientation

As one can see from Fig. 7 one obtains, as expected, the maximum crack signal in the case of an electromagnetic excitation where the eddy currents are oriented perpendicular (alpha = 90°) to the crack length orientation. This is because in this case the disturbance of the eddy currents by the crack is strongest. But also for cases where the angle between the eddy currents and the crack length is up to 60° one observes only a mild reduction of the crack signal. For an angle of 45° the signal drops down on a value of about 75% and for an angle of 30° one still finds a signal of about 50% of the maximum signal. In the case where the eddy currents are propagating parallel to the crack length (alpha = 0°) the crack signal is still nearly 30% of the maximum signal.

3.3 Application of the technique for detection of cracks in industrial components

Industrial ferritic steel components produced by forging were examined with the thermal technique using inductive and ultrasonic heating. In all of the following examples, the surface was as-received. A measurement result on a tube-shaped component using an excitation where the eddy currents were oriented perpendicular to the crack orientation is presented in Fig. 8. Fig. 8a shows a thermographic image shortly after the begin of the inductive excitation. As can be seen right of the arrow the crack is producing a clear temperature contrast along the crack length. In Fig. 8b the temperature distribution along a line indicated by the arrow is shown. Beside the contrast displaying the defect generated by the mechanisms discussed in the previous chapter, the inductive heating causes a general temperature enhancement on the surface of the cylindrical component due to the eddy current losses in the sound material.

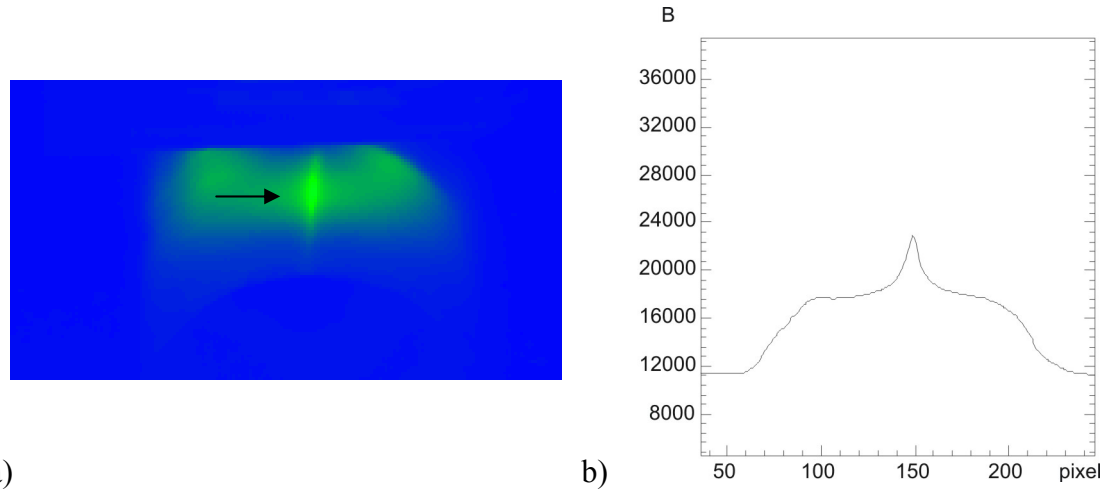

Fig. 8: a) Thermographic image of a real crack in a tube like component and inductive excitation (view along the tube in axial direction). b) Temperature distribution along the arrow direction

For comparison, the same component was examined with an ultrasonic heating technique at 20 kHz using an excitation via a sonotrode on the cylinder surface (horizontal arrow in Fig. 9a). The specimen has been rotated by 90°. With this technique the crack can be detected as well (below the vertical arrow in Fig. 9a) but not in its whole extension. Obviously a region of the crack at right of the vertical arrow produces no heat due to lack of sufficient friction energy.

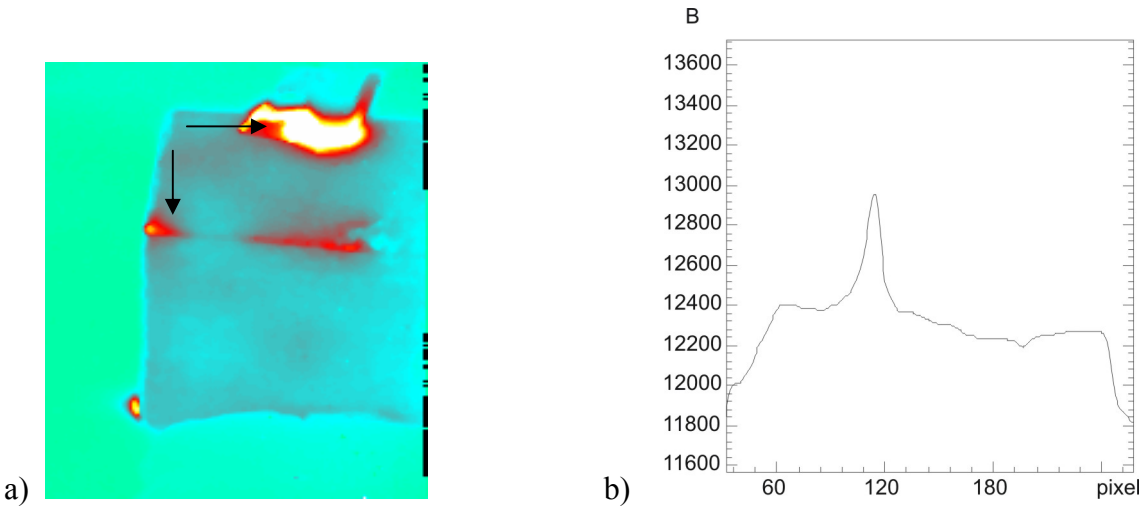

Fig. 9: a) Thermographic image of a real crack in a tube like component by ultrasonic excitation. b) Temperature signal along the vertical arrow

Many other components and geometries were investigated. A general finding was that with the given equipment, induction heating was applicable to a larger variety of specimen shapes and showed more crack indications as the ultrasonic heating technique.

For verifying the measurement results, a metallographic examination of the crack region was performed. Fig. 10 shows a metallographic cross section along the arrow direction in Fig. 8a. The crack shows an inclination angle to the surface less than 90°. Its maximum depth was measured to be about 0.4 mm.

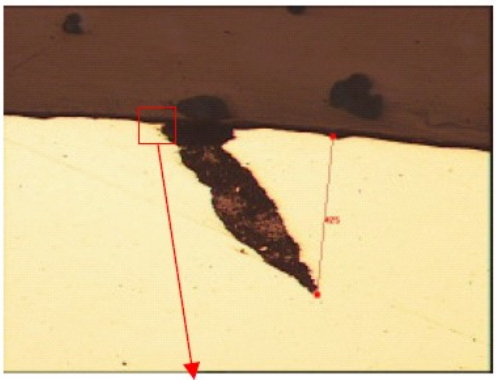

Fig. 10: Metallographic cross section along the arrow in Fig. 8a

A further application example of the inductive heating technique is presented in Fig. 11. The thermographic image (Fig. 11a) indicates clearly the crack in this steel component.

a)

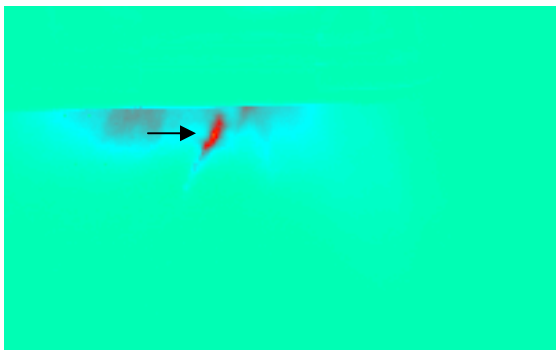

b)

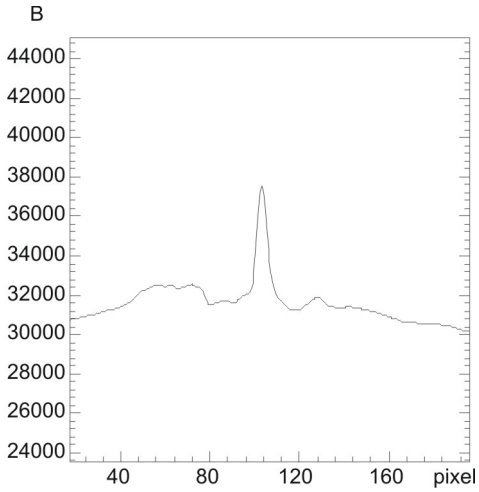

Fig. 11a: Thermographic image of a real crack in a steel component by inductive heating.
b) Temperature signal along the arrow

Again, a metallographic examination was performed for verification of the thermographic result. Fig. 12 shows a metallographic cross section along the arrow in Fig. 11a. One can recognize a crack with small inclination angle with respect to the surface. Its depth was measured to be about 0.2 mm.

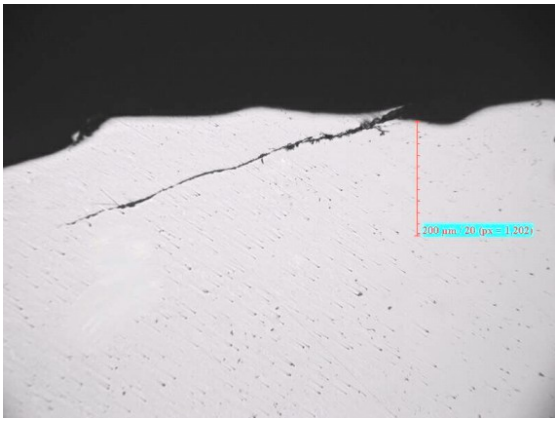

Fig. 12: Metallographic cross section along the arrow direction in Fig. 11a. The crack depth is 0.2 mm

4. Conclusions

In this contribution an analytical model was presented which allows the calculation of the temperature signal of a long crack in a ferritic steel plate due to the interaction with eddy currents produced by an electromagnetic high frequency excitation. The model predicts a linear dependence of the crack signal on crack depth up to a defect depth of about 0.8 mm. This result could be verified by experimental investigations. For defect depths larger than 0.8 mm the model and the experiments show saturation behaviour, but in the experimental results this saturation effect is stronger. This difference could be caused by the fact that in the model infinitely long cracks were considered while in the experimental investigations the crack length was 10 mm.

The signal contrast from cracks with this technique is optimal if the inductive excitation is in that way that the eddy currents are perpendicular to the crack orientation. But even at significant misalignment there remains sufficient contrast for detection. The temperature contrasts obtained were generally high and suitable for automated processing. Cracks down to 100 µm depth should be detectable. As a typical inspection time for a surface region of 10 to 100 cm^2 is less than a second, inductive heating appears to be attractive for high-speed testing of mass-production metallic components.

References

[1] K.-J. Kremer, 'Das THERM-O-MATIC-Verfahren - Ein neuartiges Verfahren für die Online-Prüfung von Stahlerzeugnissen auf Oberflächenfehler', in: "3rd European Conference in Nondestructive Testing", Florence 15- 18 October 1984, S. 171-186

[2] D. M. Heath and W. P. Winfree, Rev. Progr. Quant. Nondestr. Eval. **9**, D. O. Thompson and D. E. Chimenti (eds.), (Plenum Press New-York 1990), 577-584

[3] J. Bamberg, G. Erbeck, G. Zenzinger, 'Eddy-Therm: Ein Verfahren zur bildgebenden Prüfung metallischer Bauteile', ZfP-Zeitung **68** (1999) 60-62

[4] J. Baumann, U. Netzelmann, 'Bauteile thermographisch prüfen – Berührungsfrei, großflächig und schnell', QZ Qualität und Zuverlässigkeit **50**/9, (2005) pp. 52-58

[5] G. Riegert, T. Zweschper, G. Busse, 'Lockin thermography with eddy current excitation', QIRT Journal **1** (2004) 21-32

[6] B. Oswald-Tranta, 'Thermoinductive investigations of magnetic materials for surface cracks', QIRT Journal **1** (2004) 33-46

[7] G. Walle, M. Abuhamad, E. Toma and U. Netzelmann: 'Defect indications in sono-thermography in relation to defect location and structure', in: Proceedings QIRT Conference, Rhode Saint Genèse, Belgium 2004, pages H.20.1 - H.20.6

[8] K. Küpfmüller: “Einführung in die theoretische Elektrotechnik”, Springer Verlag: Berlin, Heidelberg, New York, 1968